Supplementary Data

Phytogenic Silver Nanoparticles Synthesized from *Dendrophthoe Falcata and Ocimum Tenuiflorum*: SERS and Ultrafast Nonlinear Optical Studies

Jhansi Mogilipuri,[1] Srilakshmi P. Bhaskar,[2] Venugopal Rao Soma,[3,*] Sabitha Mohan[1,*]

[1]Department of Physical and Chemical Sciences, Sri Sathya Sai University for Human Excellence, Navanihal, Kalaburagi, Karnataka 585313

[2]Department of Chemistry, Vimala College (Autonomous), Thrissur, Kerala 680009

[3]School of Physics and DIA-CoE (formerly ACRHEM), University of Hyderabad, Hyderabad 500046, India

Corresponding Authors email: soma_venu@yahoo.com, sabitha.m@sssuhe.ac.in

(1) TEM Micrographs

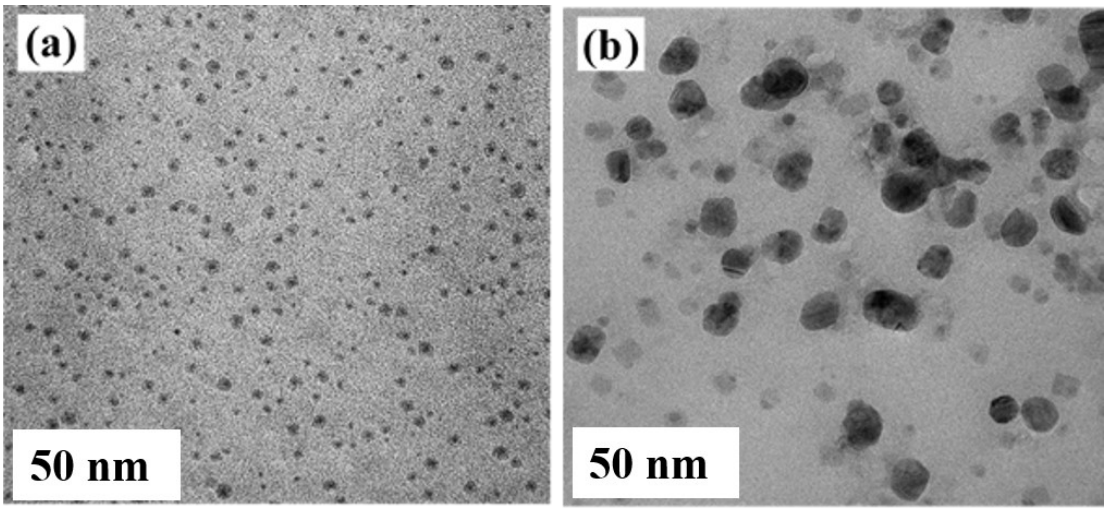

Figure S1 (a) & (b) present the TEM micrographs of AgL and AgT samples, respectively, at a resolution of 50 nm.

(2) Table 1 presenting the analytic field enhancement factors of AgL and AgT substrates

Sample	Intensity	PA [823 cm^{-1}]	NB [592 cm^{-1}]	MB [477 cm^{-1}]	CV [1618 cm^{-1}]
	I_{SERS}	222 (10 μM)	366 (10 nM)	417 (100 nM)	521 (50 μM)
AgL	I_R	128 (50 mM)	30 (1 mM)	152 (1 mM)	20 (1 mM)
	AEF	0.86×10^4	1.2×10^6	2.7×10^4	0.52×10^3
	I_{SERS}	128 (10 μM)	311(1 μM)	485 (1 μM)	177 (50 μM)
AgT	I_R	128 (50 mM)	30 (1 mM)	152 (1 mM)	20 (1 mM)
	AEF	0.5×10^4	0.1×10^5	3.19×10^3	0.17×10^3

Z-SCAN of Water

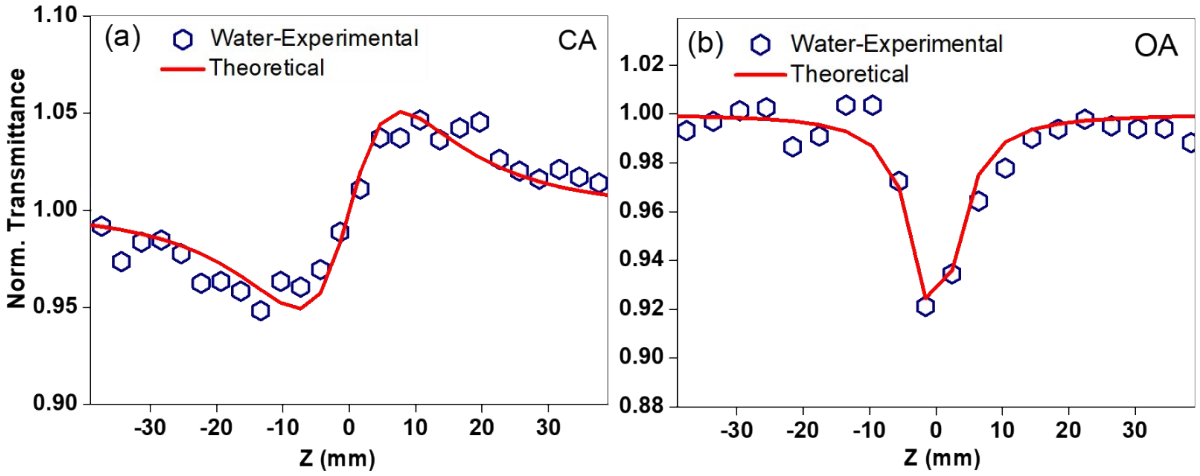

Figure S2 (a) and (b) presents the CA and OA Z-scan data of water (solvent used in the experiments), respectively.

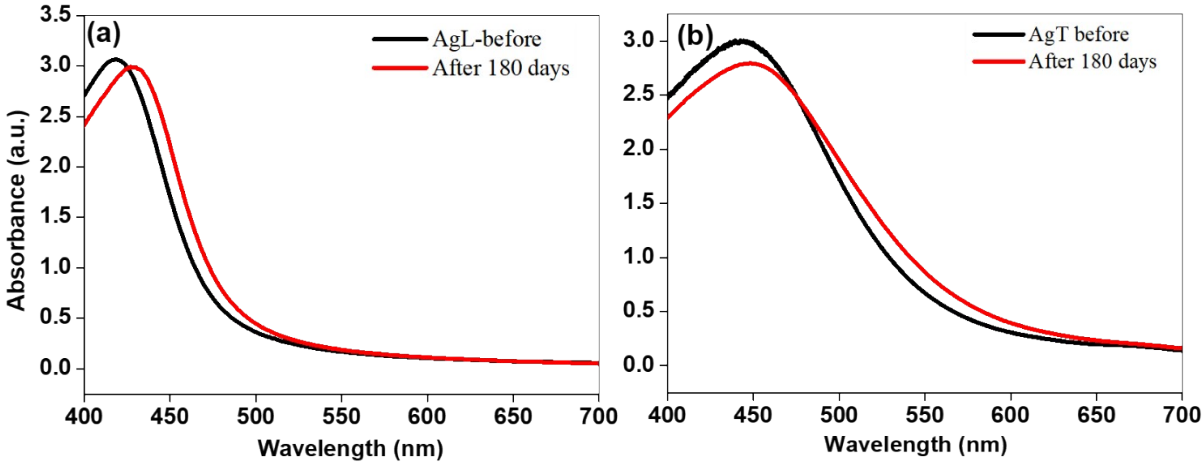

Figure S3 (a) and (b) Absorbance spectra of AgL and AgT, respectively, before (black) and after 180 days (red).

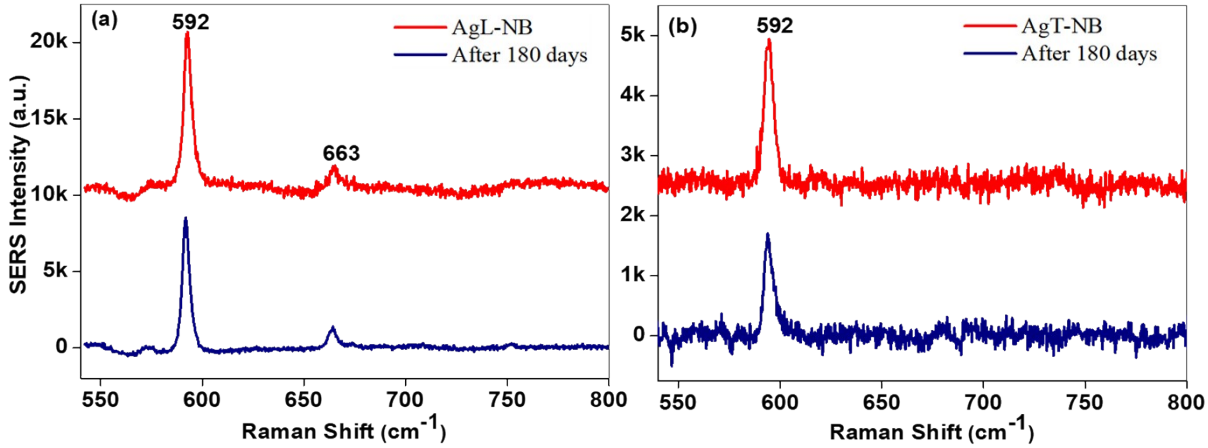

Figure S4 (a) and (b) The SERS spectra of Nile blue at a concentration of 10 µM before (red) and after (navy blue)180 days using AgL and AgT substrates, respectively

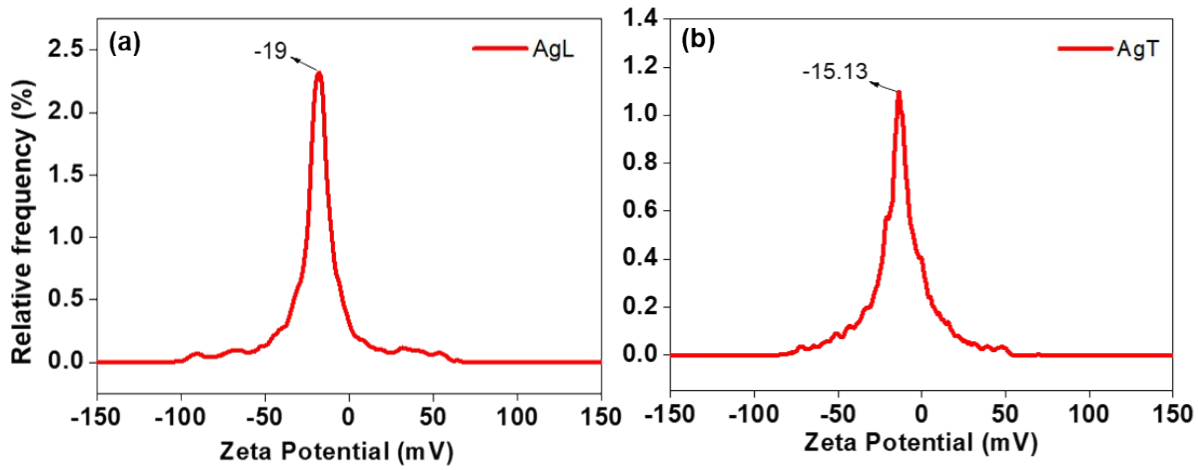

Figure S5 (a) and (b) represents the Zeta Potential measurements for AgL and AgT indicating the surface charge and colloidal stability of the respective nanoparticle systems.

Table 2: Raman modes and their assignments of NB[1,2]

S. No	Raman Shift(cm^{-1})			Peak Assignments
	Reported	Observed		
		AgL	AgT	
1	595	592	663	C-C-C and C-N-C deformations
2	673	592	663	In-plane CCC or NCC deformations

Table 3: Raman modes and their assignments of PA[3,4]

S. No	Raman Shift(cm^{-1})			Peak Assignments
	Reported	Observed		
		AgL	AgT	
1	825	823	823	CN stretching; NO_2 scissoring in-plane deformation
2	935	939	939	CN stretching; ring CCC in-plane bending In-plane CH bending
3	1338	1344	1344	NO_2 symmetric stretching

Table 4: Raman modes and their assignments of MB[5,6]

S. No	Raman Shift(cm^{-1})			Peak Assignments
	Reported	Observed		
		AgL	AgT	
1	448	445 477	447 477	Skeletal deformation of C-N-C
2	501	939		Skeletal deformation of C-N-C
3	596	596	596	Skeletal deformation of C-S-C

4	671	675	675	Out of plane bending of C-H
5	770	775	773	In-plane bending of C-H
6	890		897	In-plane bending of C-H
7	951	950	958	In-plane bending of C-H
8	1040	1030	1030	In-plane bending of C-H
9	1154	1154	1153	In-plane bending of C-H
10	1302	1304	1305	In-plane ring deformation of C-H
11	1394	1394	1394	Symmetric stretching of C-N
12	1502	1505	1507	Asymmetric stretching of C-C
13	1623	1624	1624	Ring stretching of C-C

Table 5: Raman peaks and their assignments of CV[7,8,9]

S. No	Raman Shift(cm^{-1})			Peak Assignments
	Reported	Observed		
		AgL	AgT	
1	425	418 441	423 441	Bending deformation of CNC
2	560		563	Out-of-plane deformation of CNC
3	715	728 759	726 757	Stretching CN
4	902	915	915	Bending of CCC
5	1165	1174	1174	Symmetric stretching CCC
6	1380	1371	1372	Bending CH
7	1462	1470		Asymmetric Bending CH3
8	1532	1531	1530	Stretching CN
		1591	1585	Symmetric stretching CC
9	1619	1618	1617	Symmetric stretching CC

References

(1) Bodelon, G.; Montes García, V.; Fernández-López, C.; Pastoriza-Santos, I.; Pérez-Juste, J.; Liz-Marzán, L. Bioimaging: Au@pNIPAM SERRS Tags for Multiplex Immunophenotyping Cellular Receptors and Imaging Tumor Cells (Small 33/2015). *Small* **2015**, *11*. https://doi.org/10.1002/smll.201500269.

(2) Moram, S. S. B.; Byram, C.; Soma, V. R. Gold-Nanoparticle- and Nanostar-Loaded Paper-Based SERS Substrates for Sensing Nanogram-Level Picric Acid with a Portable Raman Spectrometer. *Bull Mater Sci* **2020**, *43* (1), 53.https://doi.org/10.1007/s12034-019-2017-8.

(3) Hakonen, A.; Wu, K.; Stenbæk Schmidt, M.; Andersson, P. O.; Boisen, A.; Rindzevicius, T. Detecting Forensic Substances Using Commercially Available SERS Substrates and Handheld Raman Spectrometers. *Talanta* **2018**, *189*, 649–652. https://doi.org/10.1016/j.talanta.2018.07.009.

(4) Byram, C.; Moram, S. S. B.; Shaik, A. K.; Soma, V. R. Versatile Gold Based SERS Substrates Fabricated by Ultrafast Laser Ablation for Sensing Picric Acid and Ammonium Nitrate. *Chemical Physics Letters* **2017**, *685*, 103–107.

(5) Li, C.; Huang, Y.; Lai, K.; Rasco, B. A.; Fan, Y. Analysis of Trace Methylene Blue in Fish Muscles Using Ultra-Sensitive Surface-Enhanced Raman Spectroscopy. *Food Control* **2016**, *65*, 99–105.

(6) Pham, T. T. H.; Vu, X. H.; Dien, N. D.; Trang, T. T.; Chi, T. T. K.; Phuong, P. H.; Nghia, N. T. Ag Nanoparticles on ZnO Nanoplates as a Hybrid SERS-Active Substrate for Trace Detection of Methylene Blue. *RSC advances* **2022**, *12* (13), 7850–7863.
(7) Cañamares, M. V.; Chenal, C.; Birke, R. L.; Lombardi, J. R. DFT, SERS, and Single-Molecule SERS of Crystal Violet. *J. Phys. Chem. C* **2008**, *112* (51), 20295–20300. https://doi.org/10.1021/jp807807j.
(8) Rekha, C. R.; Sameera, S.; Nayar, V. U.; Gopchandran, K. G. Simultaneous Detection of Different Probe Molecules Using Silver Nanowires as SERS Substrates. *Spectrochimica Acta Part A: Molecular and Biomolecular Spectroscopy* **2019**, *213*, 150–158.
(9) Mandavkar, R.; Lin, S.; Pandit, S.; Kulkarni, R.; Burse, S.; Habib, M. A.; Kunwar, S.; Lee, J. Hybrid SERS Platform by Adapting Both Chemical Mechanism and Electromagnetic Mechanism Enhancements: SERS of 4-ATP and CV by the Mixture with GQDs on Hybrid PdAg NPs. *Surfaces and Interfaces* **2022**, *33*, 102175.